POLITECNICO
MILANO 1863

SPACECRAFT ATTITUDE DYNAMICS

Scarpa Edoardo 220556 10664387
Torre Federico 218640 10645141
Viola Francesco 221924 10680788
Zara Andrea 225686 10698650

Academic year 2022-2023

Contents

List of Figures

List of Tables

1 Introduction

The aim of the project is to simulate the behaviour of the assigned spacecraft during one orbit. The assigned spacecraft is a 6U cubesat that mount onboard a set of gyroscopes, two reaction wheels and one inertia wheel.

The spacecraft mission is to point towards Aldebaran, a star in the Taurus constellation, during the eclipse phase of the orbit, while charging and transmitting data to Earth during the sunlight exposure.
A reference mission taken into account is the ASTERIA (figure 1) mission that has a similar goal mission and architecture [1] compared to the case of the project. The pointing precision of the ASTERIA cubesat is about 30 arcseconds [2], for the analyzed spacecraft the precision requirements are set to 1 arcminute.

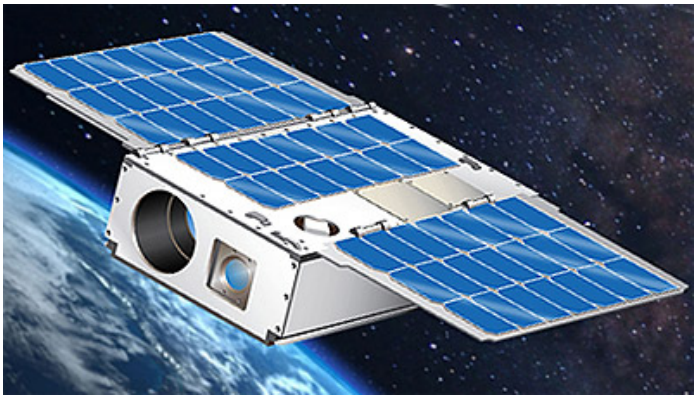

Figure 1: ASTERIA 6U cubesat

The spacecraft orbit is highly elliptical with the apocentre in the shadow cone of the Earth. This orbit has been selected to grant a longer observation period of the star than ASTERIA and reduce the disturbance magnitude. The spacecraft dynamics and the environment disturbance were modeled, in addition to the non-ideal behaviour of the sensors and the actuators. A control logic has been implemented to grant the desired pointing and to allow the switching between the different targets.

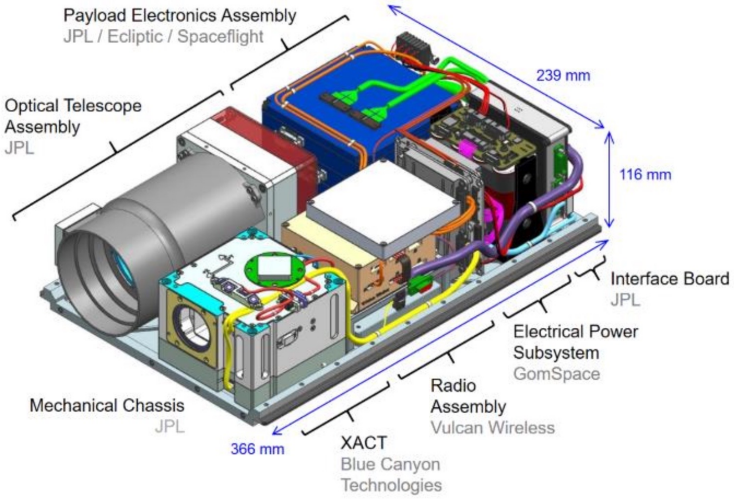

Figure 2: ASTERIA Architecture [3]

2 Architecture

Since the mission takes as reference the ASTERIA Space Telescope Mission [3], the Cube-sat has been rearranged in a similar way as the spacecraft used in the just mentioned mission. Approximately half of the internal volume is occupied from the payload, while the other half is used to carry the spacecraft bus components such as actuators, sensors, radio and electrical power subsystems.
The spacecraft x body axis is the minor inertia axis, that points in the direction of the payload, the y axis is the major inertia axis and points towards down, z axis consequently. The geometrical properties of the spacecraft are expressed in table 1.

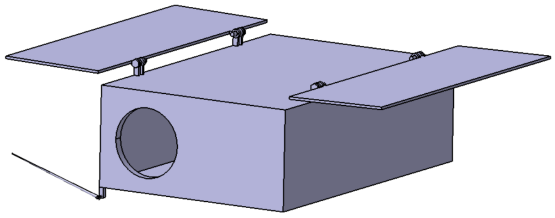

Figure 3: Cube-sat CAD model

$I_x\ [kgm^2]$	$I_y\ [kgm^2]$	$I_z\ [kgm^2]$
0.05999	0.16242	0.12530
m [kg]	Centre of mass position error [cm]	
10.2	[1, -0.5, 0.8]	

Table 1: Geometrical properties of the spacecraft [1]

2.1 Actuators

Inside the spacecraft ACDS (Attitude Control Determination System) are located three reaction wheels and an inertia wheel. These actuators, combined with sensors described below,allows the spacecraft de-tumbling and pointing in the desired direction.

2.1.1 Reaction and Inertia wheels

Reaction wheels

Reaction wheels are spinning rotors characterised by having a nominal condition with zero angular velocity. Their functioning is based on the acceleration and deceleration of the rotors which cause the exchange of angular momentum with the satellite, even without generating a net torque. Each of these actuators is driven by an electric motor, which has its typical operational curve (see *figure*4). Once the motor reaches the *saturation speed*[1], the wheel needs to be slowed down paying attention to not generate an undesired exchange of momentum. This process is called *desaturation*[2] and requires at least another actuator.
The three *selected reaction wheels* [4] are oriented as the spacecraft principal inertial axes, and are characterised by having the physical characteristics in table 2.

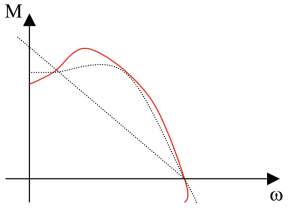

Figure 4: Electric Motor

Mass [g]	180	Dimensions [mm]	44x44x27	Inertia $[gm^2]$	300

Table 2: Physical characteristics of one reaction wheel [4]

Inertia wheels

Inertia wheel is a spinning rotor characterised by a nominal condition with a non-zero angular velocity. The chosen inertia wheel is oriented in a different direction with respect to the reaction wheels and has the same physical characteristics. Once the inertia wheel direction is defined, the following matrix can be computed:

$$A = \begin{bmatrix} 1 & 0 & 0 & \frac{1}{\sqrt{3}} \\ 0 & 1 & 0 & \frac{1}{\sqrt{3}} \\ 0 & 0 & 1 & \frac{1}{\sqrt{3}} \end{bmatrix}$$

[1] When the electric motor (and then the rotor) reaches the saturation speed, which is the maximum speed available from the electric motor, it can not provide torque anymore.
[2] The rotational speed of the rotor is decreased, so that now it can operate in the desired range of speed.

Each row of the A matrix express an orientation of the on-board actuators: the first three columns refer to the reaction wheels (oriented as the spacecraft body axes), the last one is referred to the inertia wheel orientation.

2.1.2 Magnetorquers

Magnetorquers belongs to the family of magnetic actuators, which generate a torque inducing a dipole in a coil which is surrounded by the Earth magnetic field. These actuators are involved only in desaturation process: in the studied case saturation does not occur, leaving magnetorquers **switched-off** for the whole mission duration (for this reason no magnetorquers have been included in the ACDS). The magnitude of the torque given by these actuators changes with the orbit height, accordingly with the variation of Earth magnetic field (see *section* 4.2): the provided torque is typically in the range of $10^{-3} \div 10^{-6}$Nm.

2.2 Sensors

Inside the ACDS are also located two kinds of sensors: a fiber optic gyroscope and a star sensor.

2.2.1 Fiber Optic Gyroscope

The *chosen gyroscope* [5] is a Fiber Optic Gyroscope (FOG), which functioning is described below:

1. The transmitter produces two signals in two opposite directions of the optical path (in this case the optical path is made of a fiber optic).
2. The receiver, collocated with the transmitter, will get the two signals at different time instants since they will have travelled for different lengths (gyroscope is rotating due to the spacecraft motion).
3. By knowing the time elapsed among the two signal acquisitions, it is possible to evaluate the angular velocity of the gyro.

The last measurements are made in the spacecraft reference frame, and are not affected by errors that can come from friction or motion problems. Selected FOG has the physical properties in table 3.

Mass [g]	40	Diameter [mm]	55	Thickness [mm]	17

Table 3: FOG physical properties [5]

2.2.2 Star Sensor

Star sensor is used to improve the accuracy of attitude determination. The operations needed to compute the spacecraft attitude are explained in *section 6*. In order to guarantee high precision, a star sensor must be very sensitive in terms of light intensity, but in this way undesired radiations coming from the Sun can easily deteriorate performances and the operating lifetime of the sensor. The adopted solution to this problem is to close the sensor during phases in which spacecraft attitude is not controlled, such as *de-tumbling* and *desaturation* (see sections 7.2 and 8.2). Since the mission to be accomplished consists into pointing at Aldebaran, the sensor is directed as the spacecraft x-axis, which is the same orientation of the onboard telescope. Selected star sensor is the *Standard NST* by BlueCanyon [6], which has the physical characteristics in table 4.

Mass [g]	350	Dimensions [mm]	100x55x50

Table 4: Star sensor physical properties [6]

2.3 Payload

The payload is the same used in the ASTERIA mission [1], which consists of an antenna and an optical telescope with specialized hardware to perform high-precision pointing and thermal control. Unlike the reference Cube-sat, the antenna has been oriented in the opposite direction of solar panels (which are oriented following the -$\hat{y}$ direction expressed in body frame): this aims to facilitate the achievement of the mission *phase 3* (see *section* 3.1.3).

3 Model description and Orbit parameters

The purpose of the 6U Cube-sat is to observe Aldebaran more than 20 minutes and with high accuracy. Aldebaran is a star in the constellation of Taurus. It is located 65 light-years. It is a giant star and it varies in brightness. Aldebaran it is believed to host a planet but the scientific community is divided because thanks the natural variation of magnitude of star is difficult to understand if there is a planet. In order to extinguish any doubt it is decide to use a Cube-sat [7] [8].
It is decided to use an orbit with high eccentricity in order to minimize the disturbance for attitude and maximize the time in shadow, according to the second Kepler's law. The altitude of pericenter is 500 km and it is decide that in 1 day the spacecraft have to pass the point 5 times. The apse line of orbit is aligned with the projection of star to ecliptic. In order to calculate the Kepler's parameters are used the spherical triangles.

a [km]	e	i [rad]	Ω [rad]	ω [rad]	θ [rad]
14419.9311854	0.530440893724	0.409279709592	0	4.35963757801	0

Table 5: Keplerian's Orbit Parameters

Departure date is 2023-12-1 at 12:00 figure 5b. In first approximation the effects on orbit perturbation has been neglected and it was studied the evolution of the time in shadow during 1 year period. As it is possible see in figure 5a the maximum time duration of the Cubsesat observation last 75 minutes.

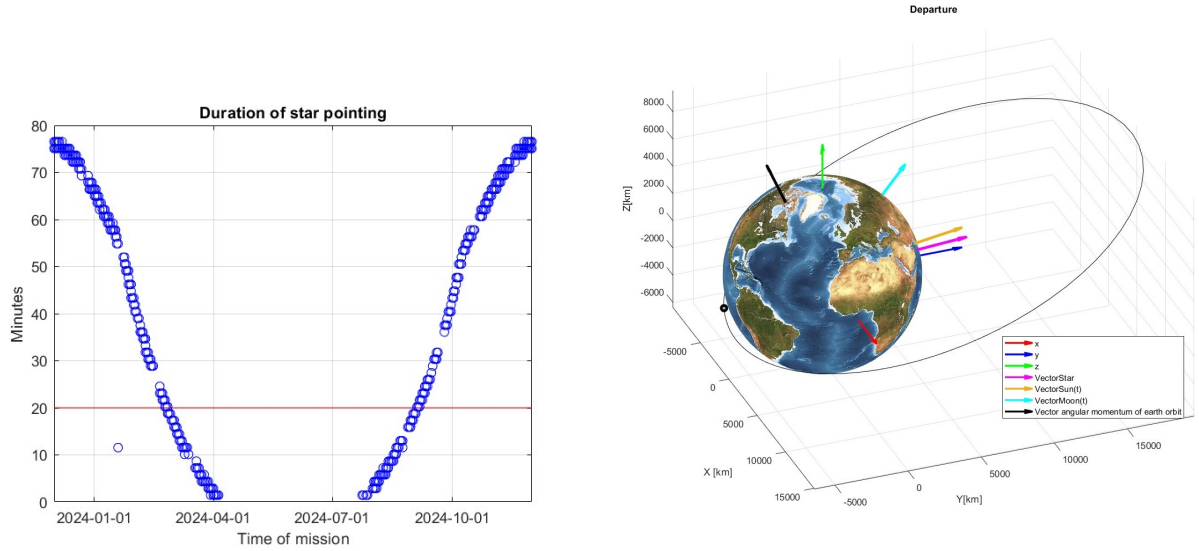

(a) Duration of star pointing

(b) Initial vectors and orbit

Figure 5: Spacecraft orbit characterization

3.1 Mission phases

During the orbit there are more pointing target:

1. Star pointing
2. Sun pointing
3. Earth pointing
4. Detumbling
5. Desaturation

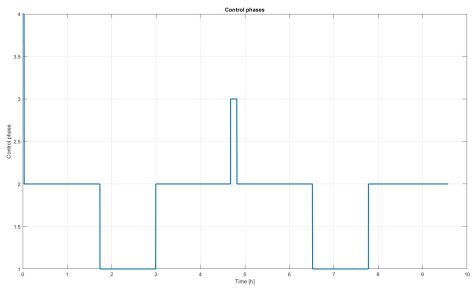

Figure 6: Control phases sequence

3.1.1 Star pointing

The main mission of the designed cubesat is the star pointing but it is possible only when:

1. The spacecraft is inside the shadow cone of the Earth.
2. The angle between moon, spacecraft and star is larger than 30 degrees [1]

In order to verify if the Cubesat is inside the shadow it is computed the angle between the SunVector and the position of spacecraft.

$$\beta = \arccos\left(\frac{VectorSun \bullet SCposition}{\|VectorSun\|\|SCposition\|}\right)$$
$$Rp_y = \|SCposition\| \sin\beta$$

The shadow is modeled as cylinder where Rp_y is smaller than 0 and β is smaller than 90 degrees. Referring to a geocentric inertial frame, VectorSun is defined as the vector going from Sun to the Earth position. Then the shadow cylinder longitudinal axis will be oriented in the same direction as VectorSun. In this case the X vector expressed in body frame has to be aligned with the star direction due to the position of the orbital telescope. Geocentric inertial coordinates of Aldebaran for x-vector have been used. Because of the star is 65 light-years distant, the maximum error due to position variation along the orbit is less than 0.2 arcseconds, therefore the pointing is considered inertial.

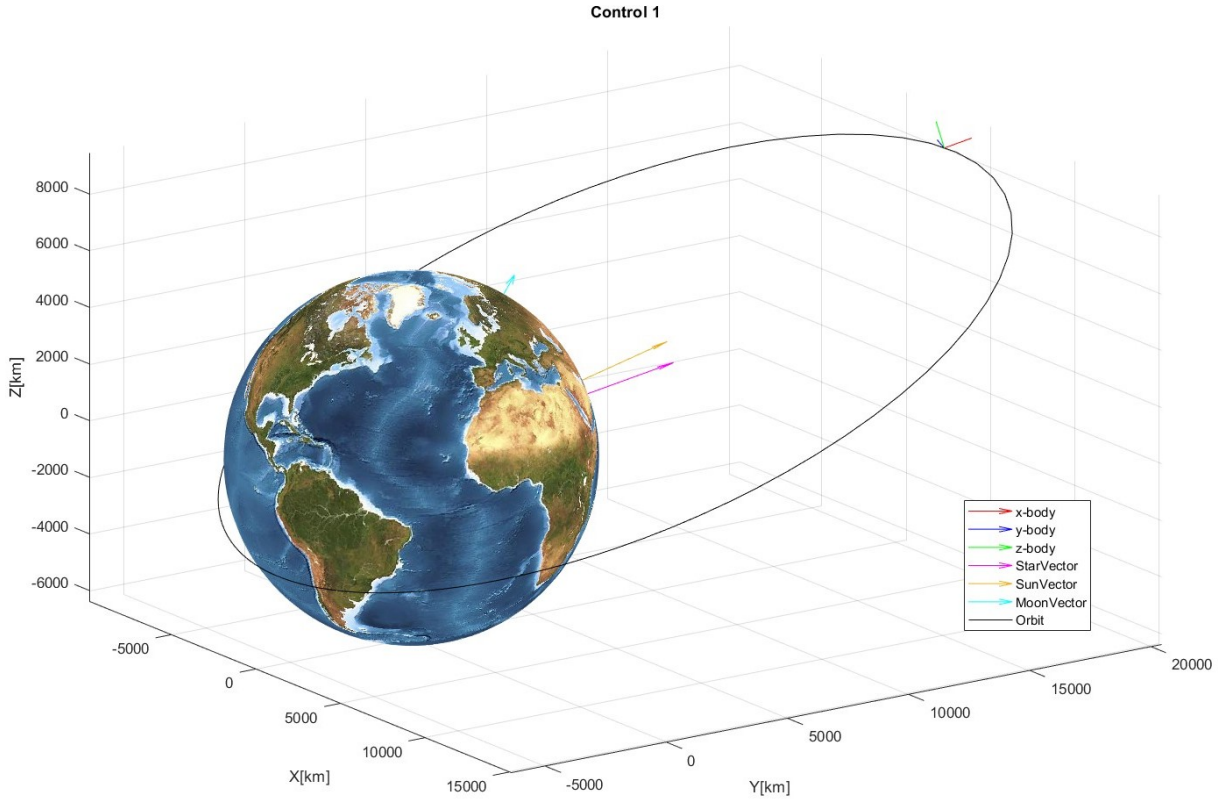

Figure 7: Spacecraft during control 1

3.1.2 Sun pointing

The second phase is sun pointing in order to recharge the spacecraft with its solar panels. In this case the cubesat must not be in shadow and the y vector must be aligned with SunVector. In fact solar panels are in the opposite direction of the y-body axis. The z-body axis must be aligned with momentum of Earth's orbit and the x-body axis is defined consequently.

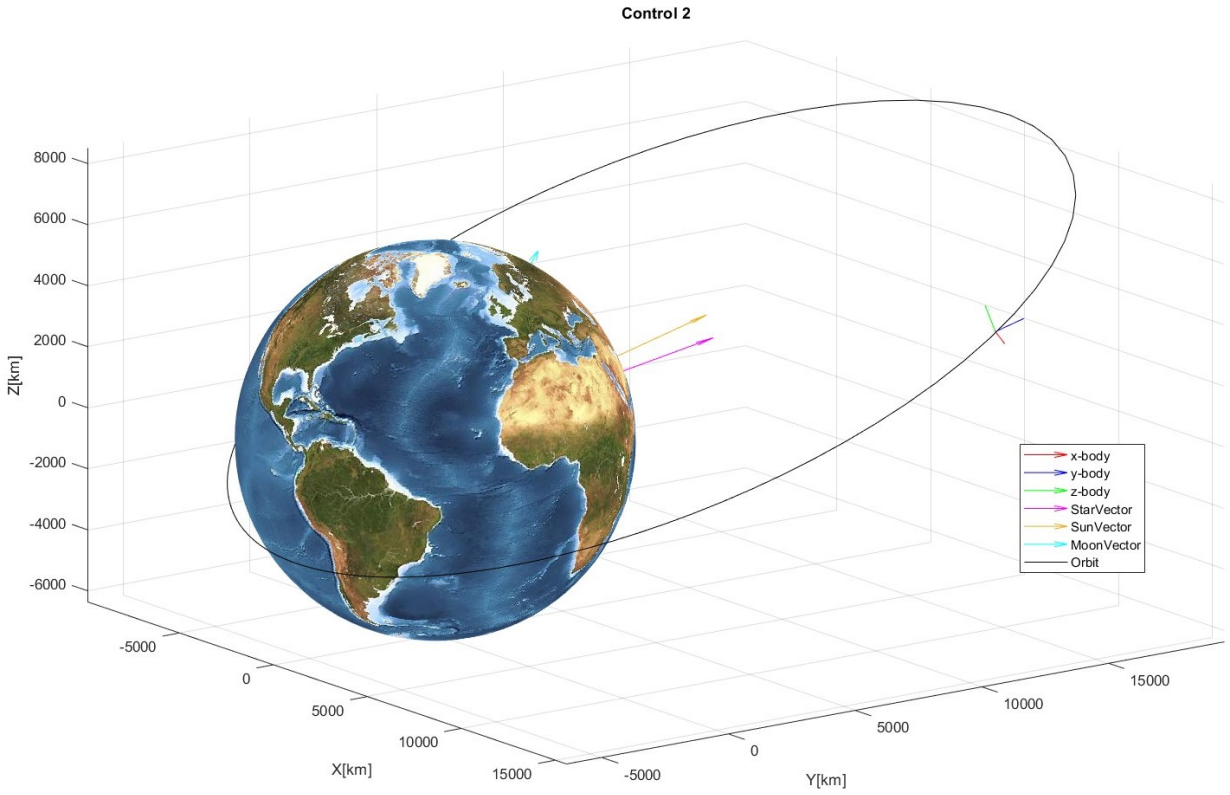

Figure 8: Spacecraft during control 2

3.1.3 Earth pointing

The last pointing phase of the mission consists in Earth pointing in order to transmit data to the ground station of New Norcia in Australia. This phase begins when latitude and longitude of Cubsat is near the ground station coordinates and the altitude is lower than the semi-latum rectus so the true anomaly of cubesat is between $-\frac{\pi}{2}$ and $\frac{\pi}{2}$. In this case the y-body vector point the ground station according to these equations:

$$\Delta Lat = latNorcia - lat$$
$$\Delta Lon = lonNorcia - lon$$

$$d = \sqrt{h^2 + \left(2 * r_E * \sin\frac{\Delta Lat}{2}\right)^2 - 2 * h * \left(2 * r_E * \sin\frac{\Delta Lat}{2}\right) * \cos\left(\frac{pi}{2} + \frac{\Delta Lat}{2}\right)}$$

$$l = \sqrt{h^2 + \left(2 * r_E * \sin\frac{\Delta Lon}{2}\right)^2 - 2 * h * \left(2 * r_E * \sin\frac{\Delta Lon}{2}\right) * \cos\left(\frac{pi}{2} + \frac{\Delta Lon}{2}\right)}$$

$$\phi = \arccos\left(\frac{h^2 + d^2 - \left(2 * r_E * \sin\frac{\Delta Lat}{2}\right)^2}{2 * h * d}\right) * sign(\Delta Lat)$$

$$\psi = \arccos\left(\frac{h^2 + l^2 - \left(2 * r_E * \sin\frac{\Delta Lon}{2}\right)^2}{2 * h * l}\right) * sign(\Delta Lon)$$

$$y_{body} = R_3(\psi)R_2(\phi) * (-x_{lvh})$$

The z-body must be perpendicular to ground station and to x_{lvh} and x-body is defined consequently.

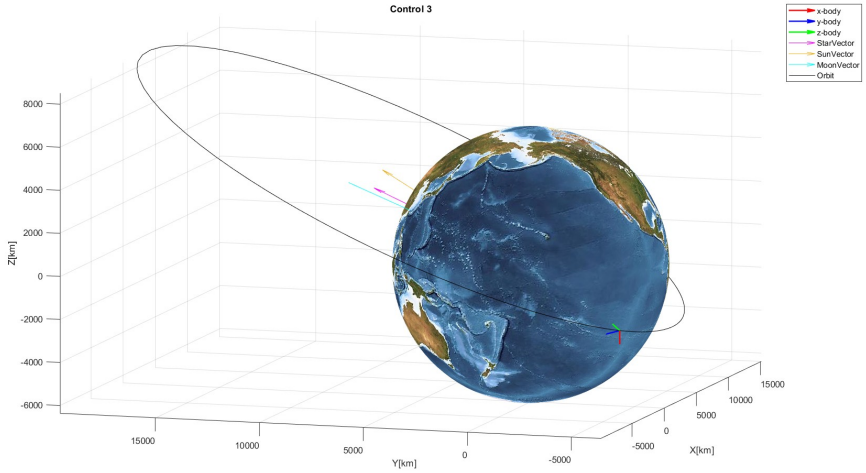

(a) Spacecraft during control 3

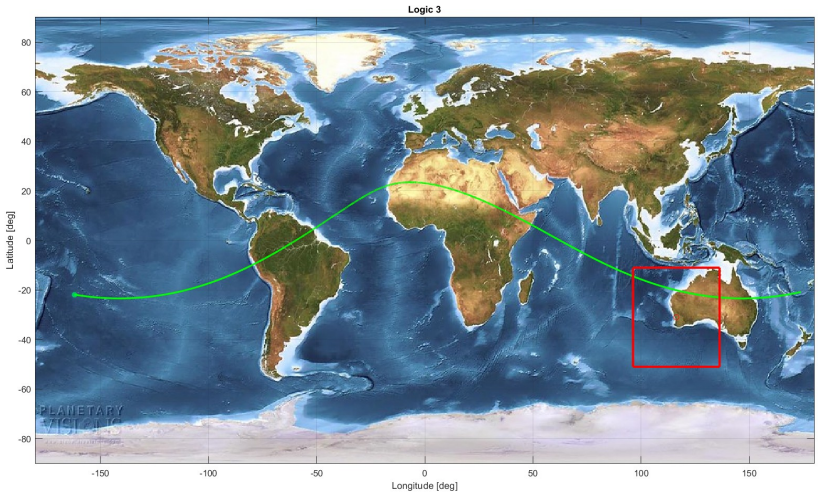

(b) Ground track

Figure 9: Phase 3 pointing

There are other two operative phases of mission: the initial detumbling and desaturation of reaction wheels.

3.1.4 Detumbling

During the de-tumbling phase the initial angular velocity of the spacecraft is driven to zero by the control action. the command persist until the error of angular rate is below a limit value.

3.1.5 Desaturation

In this project it is decide to use the reactions wheel to control the attitude of spacecraft but it is possible that during the mission the revolution per minutes of one wheel arrive ad maximum allowed. So it is necessary to report below a threshold the wheel. In order to do this it is possible to use other actuators like magnetorquers or thrusters. Desaturation mode will begin when one wheel arrive at maximum and it finish only when the angular velocity of all reaction wheels are below a limit value. During the de-tumbling phase the control of the spacecraft is not considered and the control torque is applied only if thrusters or magntorquers maximum torque is not reached with the requested torque for the desaturation.

4 Environment

During its operations, the spacecraft will be subjected to external disturbing torques: in order to define these disturbing actions, a model of the external environment is required. The disturbances taken in account are the Earth gravity gradient, the Earth magnetic field and the solar radiation pressure. The third body perturbation caused by the Moon and the atmospheric drag can be neglected because the orbit is close to the Earth, but not enough to be affected in a significant way by disturbances coming from the atmosphere.

4.1 Gravity Gradient Torque

Due to the irregularity of Earth shape, the gravity field around it won't be uniform and it can cause a torque acting on the spacecraft depending on its position (with respect to Earth) and its attitude:

$$M_x = \frac{3Gm_t}{R^3}(I_z - I_y)c_3c_2$$
$$M_y = \frac{3Gm_t}{R^3}(I_x - I_z)c_1c_3$$
$$M_z = \frac{3Gm_t}{R^3}(I_y - I_x)c_2c_1$$

Since this force is generated by the same force field which causes the orbit motion, it will be continuously acting on the spacecraft. By substituting the gravity gradient torque expression inside the Euler equation, the following relations are obtained:

$$\begin{cases} I_x\dot{\omega}_x + (I_z - I_y)\omega_z\omega_y &= \frac{3Gm_t}{R^3}(I_z - I_y)c_3c_2 \\ I_y\dot{\omega}_y + (I_x - I_z)\omega_x\omega_z &= \frac{3Gm_t}{R^3}(I_x - I_z)c_1c_3 \\ I_z\dot{\omega}_z + (I_y - I_x)\omega_y\omega_x &= \frac{3Gm_t}{R^3}(I_y - I_x)c_2c_1 \end{cases}$$

where c_1, c_2 and c_3 are the direction cosines of the radial direction in body axes.

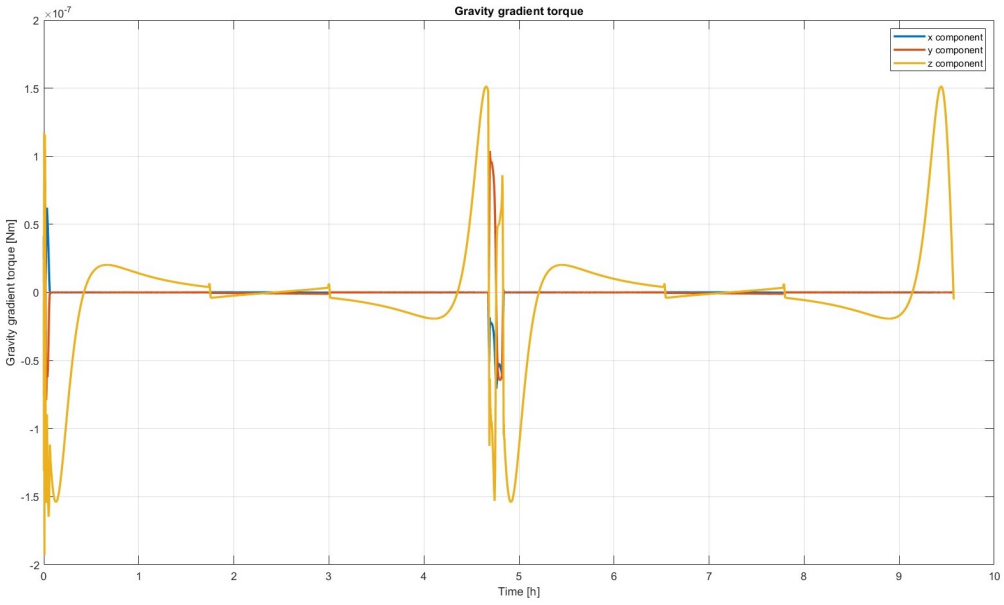

Figure 10: Gravity gradient perturbation over 2 periods

4.2 Magnetic Torques

The Earth magnetic field can be compared to that generated by a dipole inclined by about 11.5 degrees referring to Earth rotation axis. In contrast with Earth gravitational field, the magnetic one is not constant considering that it slowly rotates and reduces its amplitude in time. The magnetic field potential function has been modeled as a series expansion of spherical harmonics:

$$V(r,\theta,\psi) = R\sum_{n=1}^{k}\frac{R^{n+1}}{r^{n+1}}\sum_{m=0}^{n}(g_n^m\cos(m\psi) + h_n^m\sin(m\psi))P_n^m(\theta)$$

where R is the Earth equatorial radius, (r,θ,ψ) are the spherical coordinates of the spacecraft position, g_n^m and h_n^m are time-dependent coefficients obtained experimentally up to the 13^{th} order [9]. Once the potential has been defined, magnetic field components can be written as:

$$B_r = \frac{-\delta V}{\delta r} \qquad \longrightarrow radial$$
$$B_\theta = \frac{-1}{r}\frac{\delta V}{\delta \theta} \qquad \longrightarrow elevation$$
$$B_\psi = \frac{-1}{r\sin\theta}\frac{\delta V}{\delta \psi} \qquad \longrightarrow azimuth$$

Once magnetic field components are obtained, it is possible to evaluate the torque acting on the spacecraft:

$$\underline{M} = \underline{m} \wedge \underline{B} \tag{1}$$

where **m** (expressed in $[Am^2]$) is the residual magnetic induction due to currents inside the spacecraft: in most of the cases this is an undesired effect coming from the parasitic magnetic induction. In other cases, magnetic actuators (which exploit this effect) may be used in order to obtain a control torque.

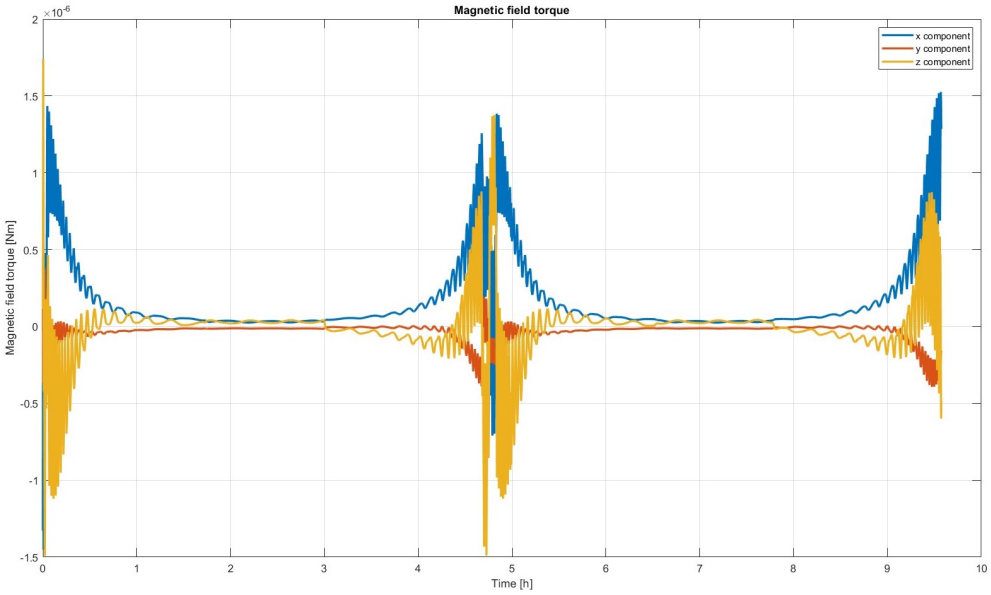

Figure 11: Magnetic field perturbation over 2 periods

4.3 Solar Radiation Pressure

The radiation coming from the Sun exerts a pressure on the enlighted faces, which in turn becomes a force acting on the spacecraft outer surface. The average pressure due to radiation has been evaluated as:

$$P = \frac{F_e}{c}$$

where c is the speed of light in the vacuum and $F_e = 1358\frac{W}{m^2}$ is the power per unit surface. Depending on the kind of external surface of the spacecraft the radiation can behave in three different ways, and this affects also the produced force. Following are reported the forces expressions referred to the surface element dA having orthogonal direction $\hat{N}$:

$$d\underline{F}_{absorbed} = -P\rho_a \cos\theta \cdot \hat{S} dA$$
$$d\underline{F}_{diffused} = P\rho_d \left(-\frac{2}{3}\cos\theta \cdot \hat{N} - \cos\theta \cdot \hat{S}\right) dA$$
$$d\underline{F}_{specular} = -2P\rho_s \cos^2\theta \cdot \hat{N} dA$$

where $\hat{S}$ represents the unit direction of the satellite-Sun vector and θ is the angle between $\hat{N}$ and $\hat{S}$. Note that if θ is greater than 90 degrees the surface is not illuminated and then not subject to solar radiation pressure. Moreover, the coefficients ρ_s, ρ_d and ρ_a are such that:

$$\rho_s + \rho_d + \rho_a = 1$$

By rearranging these coefficients, the following relation can be obtained:

$$\rho_s + \rho_d = 1 - \rho_a$$

Then, the expression of the force acting on the spacecraft due to SRP becomes:

$$\underline{F}_i = -PA_i(\hat{S}_B \cdot \hat{N}_{Bi}) \left[(1-\rho_s)\hat{S}_B + \left(2\rho_s(\hat{S}_B \cdot \hat{N}_{Bi}) + \frac{2}{3}\rho_d \right) \hat{N}_{Bi} \right]$$

where $\hat{S}_B$ and $\hat{N}_{Bi}$ are respectively the the unit direction of the satellite-Sun vector measured in body frame and the normal for each external surface of the spacecraft in body frame. Once the force has been evaluated, the solar radiation pressure torque can be computed as:

$$\underline{M}_{SRP} = \sum_{i=1}^{n} \underline{r}_i \wedge \underline{F}_i$$

where $\mathbf{r}_i$ is the position of the centre of pressure of the i-th spacecraft surface with respect to the centre of mass. The expression of the torque above is true only if $\hat{S}_B \cdot \hat{N}_{Bi} > 0$ which equals to say that the i-th surface is illuminated. Otherwise, if $\hat{S}_B \cdot \hat{N}_{Bi} < 0$, the contribution of the i-th surface is equal to 0 (it is not hit by the radiation).

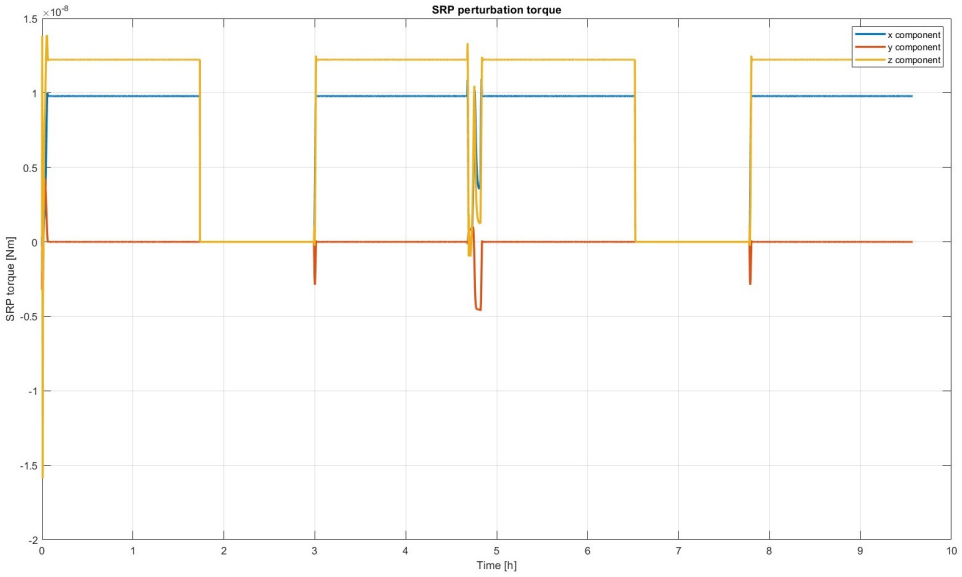

Figure 12: Solar radiation pressure perturbation over 2 periods

5 Model of spacecraft dynamics

To simulate the spacecraft behaviour during one orbit of the mission, a model of its dynamic response and its kinematics is needed.

5.1 Spacecraft dynamics

The spacecraft dynamics model follows the Euler equations, which equals the variation of total angular momentum expressed in the inertial frame to the external torque applied to the spacecraft.

$$\dot{\underline{h}}_N = \dot{\underline{h}}_B + \underline{\omega} \wedge \underline{h}_B = \underline{M}_{ext}$$

The body frame axes are assumed to be principal of inertia and centered in the spacecraft centre of mass. Denoting I_x, I_y and I_z the principal inertia moments and writing ω in the body frame as $\underline{\omega}_B = [\omega_x, \omega_y, \omega_z]^T$, the Euler equations can be rewritten as:

$$\begin{aligned} I_x\dot{\omega}_x + (I_z - I_y)\omega_z\omega_y &= M_x \\ I_y\dot{\omega}_y + (I_x - I_z)\omega_x\omega_z &= M_y \\ I_z\dot{\omega}_z + (I_y - I_x)\omega_y\omega_x &= M_z \end{aligned}$$

Dual-spin dynamics and reaction wheels

The reaction wheels mounted onboard the spacecraft exchange angular momentum with the spacecraft itself during the control action. This exchange in momentum can be modeled, according to the wheels dynamics, modifying the Euler equation written above. The whole system dynamic is schematized below, considering a set of four wheels of inertia I_w and collecting the components of each rotation axis, expressed in the body frame, in the columns of the matrix A.

$$\begin{gathered} \dot{\underline{h}}_B + \dot{\underline{h}}_w + \underline{\omega} \wedge \underline{h}_B + \underline{\omega} \wedge \underline{h}_w = \underline{M}_{ext} \\ I_w\underline{\omega}_w = \underline{M}_w \\ where\ \underline{h}_w = AI_w\underline{\omega}_w \end{gathered}$$

5.2 Spacecraft kinematics

The kinematic model of the spacecraft was implemented using the Euler Angles formulation. In particular the sequence adopted for the rotation axes is 312. The kinematics relations are differential equations that represent the evolution of the spacecraft attitude according to the temporal variation of the angular velocity. For the chosen sequence, denoting ϕ, θ and ψ the magnitudes of the rotations referred to the first, second and third rotation respectively, are expressed below:

$$\begin{aligned} \dot{\phi} &= \frac{\omega_z \cos\psi - \omega_x \sin\psi}{\cos\theta} \\ \dot{\theta} &= \omega_x \cos\psi + \omega_z \sin\psi \\ \dot{\psi} &= \omega_y - (\omega_z \cos\psi - \omega_x \sin\psi)\frac{\sin\theta}{\cos\theta} \end{aligned}$$

Singulatity condition

As visible from the previous equations, the 312 sequence has a singularity when the cosine of the second angle tents to zero, so when $\theta \to \pm\frac{\pi}{2}$. In order to remove the singularity the kinematic model is enforced to switch to the axes sequence 313 when the second angle goes near the singular point. The alternative sequence of rotation has a different singular point, where the sine of the second angle goes to zero. Switching between the two sequences the singularities can be avoided. This process brings an additional computational cost to the simulation but it is requested only during the de-tumbling phase and the slew manoeuvre, where the attitude variation is large.

6 Sensors

To detect the behavior of the spacecraft and its relation with the environment the spacecraft is provided with sensors:
In particular are used [5] [6]:

Type	Manufacturer	Sensor model
Star sensor	Blue Canyon Technologies	Standard NST
Gyroscope	Fizoptika Malta	FOG VG103S-2LND

Table 6: Onboard sensors

6.1 Star sensor

Star sensors allow the measurement of the spacecraft attitude by comparison of the detected stars, in terms of light intensity and radiation spectrum, with a map of stars on board the sensor.
Star sensors performs four operations:

1. Data acquisition
2. Correct position in space of acquired data
3. Identification of stars from a star catalogue
4. Attitude determination

During the pointing phases the star sensor is always operative because the spacecraft x axis, along which the sensor is mounted, never points towards the Sun or the Earth. Instead, during the de-tumbling and desaturation phases the star sensor is switched off to avoid the damaging of the instrument if exposed to direct sunlight.

Simulink model

To model the attitude measurement of the star sensor some disturbances are applied to the real Direction Cosine matrix of the spacecraft. The characteristics of the chosen star sensor are expressed in table 7.

Sampling frequency [Hz]	Cross sensitivity [arcsec]	About sensitivity [arcsec]
5	1	10

Table 7: Star sensor parameters

The disturbance has been modeled as random Gaussian process of standard deviation given by the cross sensitivity for the rotation angles around the y and z axes and by the about sensitivity for rotation around x axis. Once computed the three amplitudes a rotation matrix for small angles is built and premultiplied to the unperturbed one. An additional source of error is caused by misalignment of the sensor in the assembly of the spacecraft. However for the aim of the project this error has been neglected. As represented in figure 13 during the initial phase, when the star sensor is switched off, the attitude error is larger while when the star sensor is operative the error is very small.

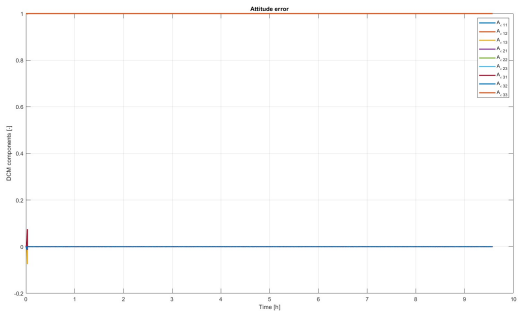

Figure 13: Error in the attitude measure

6.2 Gyroscope

Gyros are used to measure angular velocity of the spacecraft. There are different types of gyros: Mechanical,Piezoelectric,Fiber Optic gyro.
The fiber optic gyro measure the angular velocity in a reference frame fixed with the satellite, in addition its not subject to friction and motion problems.
The gyroscopes in general has problem due to noise and bias disturbance. In the following section is illustrated how its been model the gyro by considering this errors.

Simulink model

The real angular rate $\underline{\omega}$, computed in the spacecraft dynamics model (Section 5) is the input of the gyroscope model. A real gyroscope is characterized by some disturbances, the main errors are the white noise $\underline{n} = \sigma_n \zeta_n$ and the bias error $\dot{\underline{b}} = \sigma_b \zeta_b$. The perturbed angular velocity can be modelled as:

$$\underline{\omega}_M = \underline{\omega} + \underline{n} + \underline{b}$$

The noise disturbance $\underline{n}$ corresponds to a random Gaussian process, attributed to thermo-mechanical noise of the system, of standard deviation given by $\sigma_n = ARW/\sqrt{T_s}$ and zero mean. The Angular Random Walk (ARW) is a parameter expressed in the gyroscope datasheets, while T_s is the sampling time of the gyroscope. The bias disturbance $\underline{b}$ is the integral of a random Gaussian process of zero mean and standard deviation related to the Rate Random Walk (RRW) of the gyroscope. In the considered datasheets the value of the RRW is not present but can be computed from the bias instability: $RRW = \frac{bias\,instability}{\sqrt{T_s}}$. The standard deviation of the bias derivative is than $\sigma_b = RRW/\sqrt{T_s}$.

The white noise disturbance can be filtered over time using a low-pass filter if necessary. The selected fiber optic gyroscope is characterized by a very low noise value, therefore the filtering is not applied. For another consulted fiber optic gyroscope [10] the relevant white noise needs filtering to reduce the disturbance magnitude. However the filter can introduce a delay in the measurement, additional source of error, especially when the variation of angular rate is high.

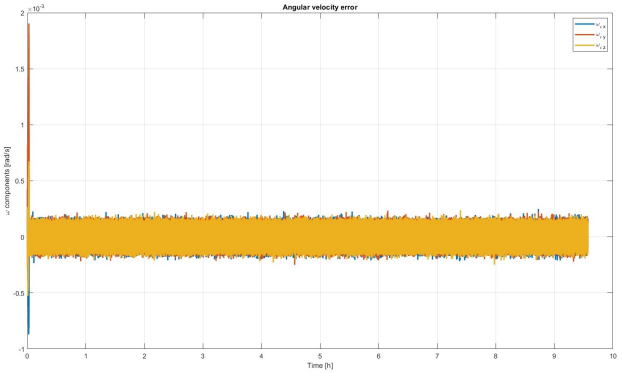

Figure 14: Error in angular rate measure

The bias disturbance cannot be filtered but the gyroscope can be reset each time another measurement of angular rate occurs. When the onboard star sensor is operative, every time the attitude is sampled, the bias error is canceled and the integration process start again from zero value. The selected gyroscope is characterized by a high bias error, therefore a frequent reset is needed, every time the star sensor provides a measurement. During the de-tumbling phase, where the star sensor is switched off and the bias disturbance is not reset, the error in the angular rate is higher as noticeable in figure 14. Instead when the star sensor is operative the main error contribution is the white noise. For the chosen gyroscope some parameters are expressed in table 8.

Sampling frequency [Hz]	$\sigma_n\,[rad/s]$	ARW [°/$\sqrt{}$ h]	$\sigma_b\,[rad/s^2]$	Bias instability [°/h]
250	3.2 e-5	0.007	1.2 e-3	1

Table 8: Gyroscope parameters

7 Actuators

The actuators block is defined by using five subsections, one for each phase (see Sec. 3.3.1). The spacecraft is provided by three reaction wheels and one inertia wheel (2.1.1). The actuators has to provide the control torque $\underline{M}_c$ requested from spacecraft control to work properly. The requested control torque can bring the reaction wheel to saturation: in this specific case the spacecraft does not reach this condition, so no further actuators are required. For completeness the logic to desaturate the reaction wheels through the use of magnetorquers will be described in the next subsection.

Reaction wheels

As explained in the section above the actuator have to exchange the requested torque $\underline{M}_c$ with the spacecraft. Upon the determination of the control torque required $\underline{M}_c$, the requested torque $\underline{M}_r$ (torque reaction wheels) is:

$$\underline{h}_r = \underline{M}_r = -A^*(\underline{M}_c + \underline{\omega} \wedge A\underline{h}_r)$$

Where the matrix A^* is the pseudo inverse of the matrix defined in the section (2.1.1). If $\underline{M}_r$ is higher than maximum momentum that reactions wheels are able to exchange with the spacecraft, the reaction wheels goes in saturation. In the actuators block of the Simulink model its been implemented a logic to be sure that the reaction wheels does not go to saturation. In the next section is explained the logic to control that $\underline{M}_r < \underline{M}_{rmax}$ ($\underline{M}_{rmax}$ by data sheet).

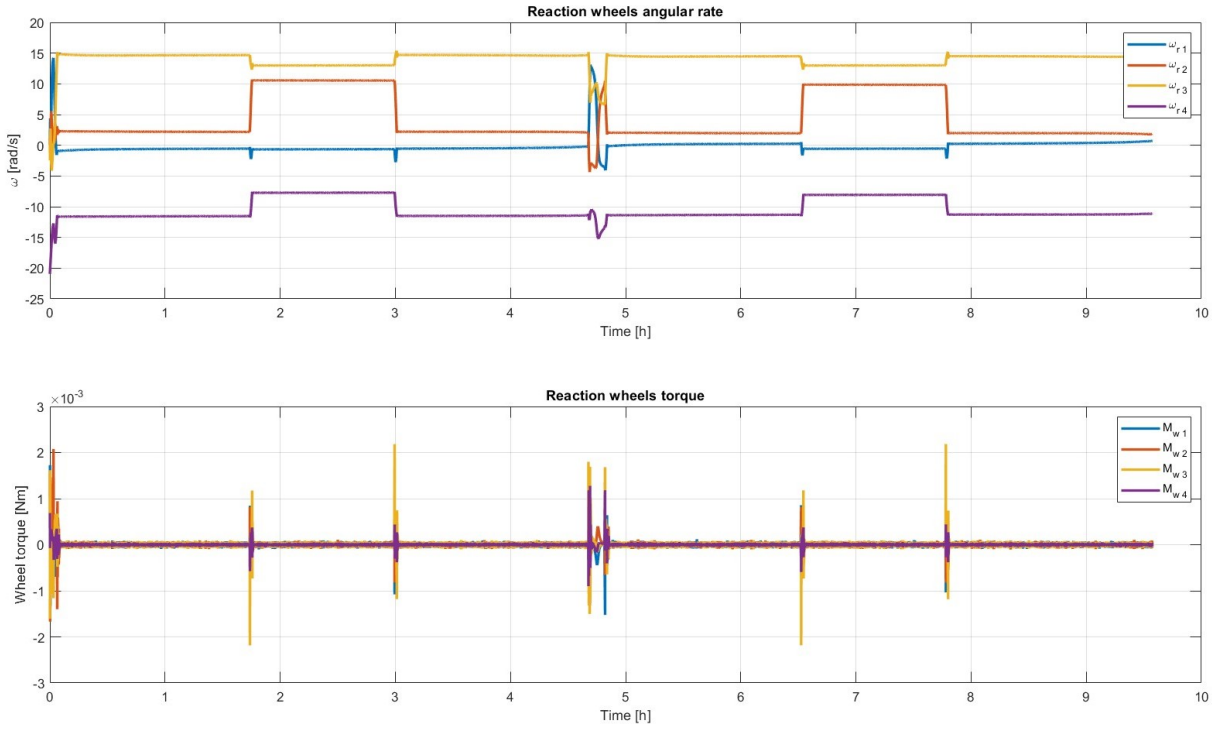

Figure 15: Reaction wheels torque

7.1 Actuators logic

The mission is divided in four phases:

- Star pointing
- Sun pointing
- Earth pointing
- De-tumbling
- Desaturation if requested

For the first four phases are used the reaction wheels to satisfy the requests of the spacecraft control. The logic implemented to avoid that the control torque is higher than maximum torque of the reaction wheels is expressed in table 9. Through this control, as visible from figure **??**, the reaction wheels torque is always

Logic	control	Output
if	$M_c - M_{maxwheel} > 0$	$M_{maxwheel}$
if	$M_c - M_{minwheel} < 0$	$M_{minwheel}$
else	$- - - - - -$	M_c

Table 9: Actuators control logic

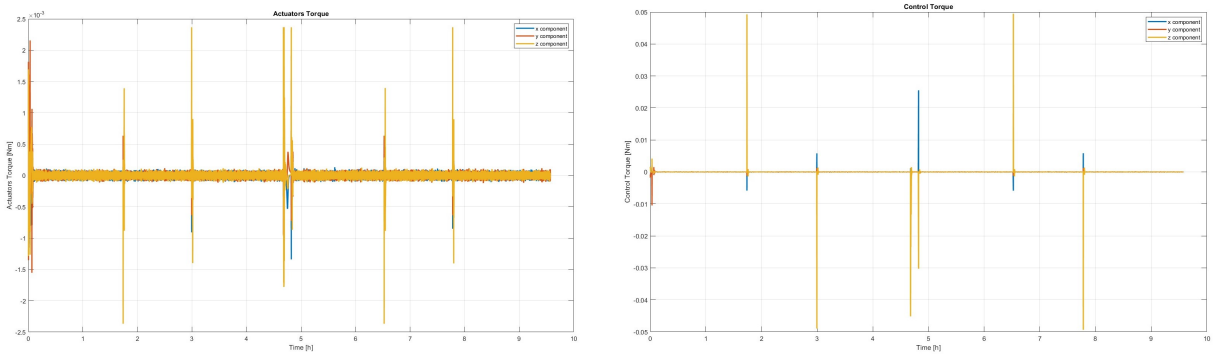

(a) M_r supplied by reaction wheels

(b) Requested M_c

Figure 16: Actuators and control torque comparison

compatible with their limits. The fifth phase request a sophisticated logic to be implemented therefore will be treated in depth in the next subsection.

7.2 Desaturation

As written before it is possible that one wheel angular momentum saturates during the orbit. In this case it is necessary to desaturate all the wheels with other actuators such that magnetorquers or thrusters. From the angular velocity is possible to compute the $\dot{\omega}$ needed to desaturate each wheel.
A proportional value is used because the request torque is very high and the desaturation proceeds slower. It is verified that the requested torque is less than the torque available from each wheel motor. At this point is necessary calculate the requested torque for each external actuator, obtained by multiplying for the matrix A the torque along the axis of each reaction wheel. If the torque requested is less than the available external actuator torque the remaining part can be used for attitude control. Otherwise it is necessary to calculate the excess torque and re-distribute this excess among the four wheels.

7.3 Magnetorquers

In case of saturation of the reaction wheels magnetorquers can be used. Magnetic actuators generate a torque that is dependent on Earth's magnetic field. For example in the table 10 is reported an possible choice of magnetorquers.

Type	Imax [mA]	Magnetic moment$[Am^2]$
Magnetorquers	150	1.9

Table 10: Magnetorquers parameters

The magnetic dipole can be modelled as:

$$\underline{D} = \mu n \underline{b}$$
$$\underline{D} = \mu \times n \times S\underline{I}$$

Where (μ) is the magnetic permeability,(n) number of windings,(S) area of coil,$(\underline{I})$ is the current intensity. The torque obtained from magnetorquers can be express as:

$$\underline{M} = \underline{D} \wedge \underline{B}$$

Due to this definition it is never possible to define three independent components of the control torque, due to this problem is used an approximate solution to define D:

$$\underline{B} \wedge \underline{M} = \underline{B} \wedge (\underline{D} \wedge \underline{B})$$

With this alternative solution we can assume that D is always perpendicular to B .

$$\underline{B} \wedge \underline{M} = \underline{B}^2 \underline{D}$$

The effective momentum that the magnetorques can exchange with the spacecraft

$$\underline{M}_{eff} = \frac{1}{B^2} (\underline{B} \wedge (\underline{M}_c \wedge \underline{B}))$$

Also magnetorquers has a maximum and minimum torque, that can be applied on the spacecraft or used to desaturate the reaction wheels,heavy influenced by the magnetic filed level. Due to this dependence from Earth's magnetic field the maximum moment is not constant and has to be calculate for each position of the spacecraft on the orbit.

7.4 Disturbances of actuators

Also actuators has mechanical disturbances generated from environment. The Simulink model is projected by defining a proportional disturbance comparing with required required torque . These errors are random errors that are multiplied by the percentage of required torque required over the maximum momentum available $(\frac{Mwheel}{Mmaxwheel})$. To fully define the random block of the disturbances has to be defined a sample time, for each actuator (reaction wheels, magnetometer), equal to the sample time of the gyroscope Instead the variance as consequence of accuracy available in the data sheets.

8 Control logic

The selected mission specifications, due to changing in the target and high precision pointing, require a three-axis control. Passive stability is incompatible with the desired change in target attitude along the orbit, because unable to manoeuvre between the different pointing phases. Therefore a PD controller has been characterized.

8.1 PD control characterization

The control logic adopted follows a Proportional-Derivative control action. The control torque is computed given an error with respect to a target condition. The proportional part is related to attitude parameters, in particular to the Direction Cosine Matrix, measured with the onboard star sensor. The attitude error matrix is given by $A_\epsilon = A_{B/N} A_D^T$, where A_D is the desired Direction Cosine Matrix for the considered mission phase. The derivative part is related to angular velocities, measured with the Fiber Optic Gyroscopes. The angular rate error is given by $\omega_\epsilon = \omega_D - \omega_B$, where ω_D is the desired angular velocity vector.
The computed control torque is proportional to the two errors through two coefficients denoted K_p and K_d, the first for the proportional part, the second for the derivative one. The selected coefficients for each mission phase are expressed in table 11. Each coefficient is obtained from the ratio of the maximum torque the actuators can give and the expected error in each mission phase.

	De-tumbling	Slew manoeuvre	Inertial pointing	Earth pointing
K_p	0.0003	0.05	0.3	0.025
K_d	0.0037	0.03	0.075	0.0500

Table 11: Proportional and derivative coefficients for each mission phase

Weight parameter

The control torque is the weighted sum of the two torques related to attitude and angular rate error. The weight parameter gives more importance to the control of attitude or of angular velocity. The sum of the two weights is equal to 1 to reach the maximum actuators torque. The derivative part weight is obtained from the ratio of the measured angular velocity magnitude and a fixed limit of admissible angular velocity (figure 17b), different for each phase (table 12), with maximum value 1, while the proportional part weight is the remaining part to one.

	De-tumbling	Slew manoeuvre	Inertial pointing	Earth pointing
ω_{lim}	0.01	0.025	0.003	0.07

Table 12: Admissible value of angular rate [rad/s]

8.2 Control phases

De-tumbling

During the de-tumbling phase the angular rate magnitude is higher than the admissible angular velocity expressed in table 12, therefore the weight parameter of the derivative part is equal to 1 (and the proportional equal to 0) (figure 17b). The control drives the angular rate to zero during this phase (figure 17a). As soon as the magnitude of the angular velocity falls under the set limit the de-tumbling phase is concluded.

Slew manoeuvre

During the slew manoeuvre the spacecraft must follows a controlled rotation to reach the desired attitude. The angular velocities have to be small but not zero (figure 18). The weight parameters oscillate around 0.5 in order to rotate the spacecraft towards the target with a small angular velocity. Once near the target attitude the slew manoeuvre control damp the system oscillation, than the slew phase is concluded.

Pointing phases

During the pointing phases the control action must keep the desired pointing within the fixed pointing accuracy. In the inertial pointing the desired angular rate is zero, therefore the derivative part weight is small

and the proportional part one is near 1. In the Earth pointing phase instead the desired angular velocity is not zero. Increasing the admissible angular rate value the proportional part is always predominant. The spacecraft follows the moving target keeping a non zero angular velocity.

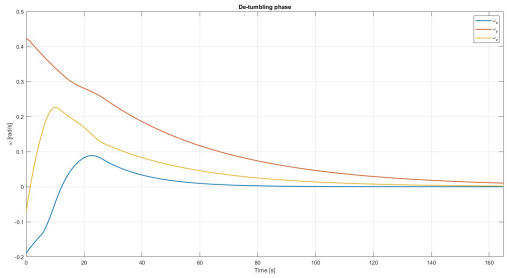

(a) ω components during de-tumbling

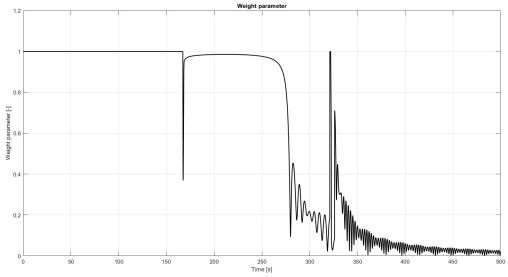

(b) Weight parameter variation

Figure 17: Control behaviour during de-tumbling and slew manoeuvre

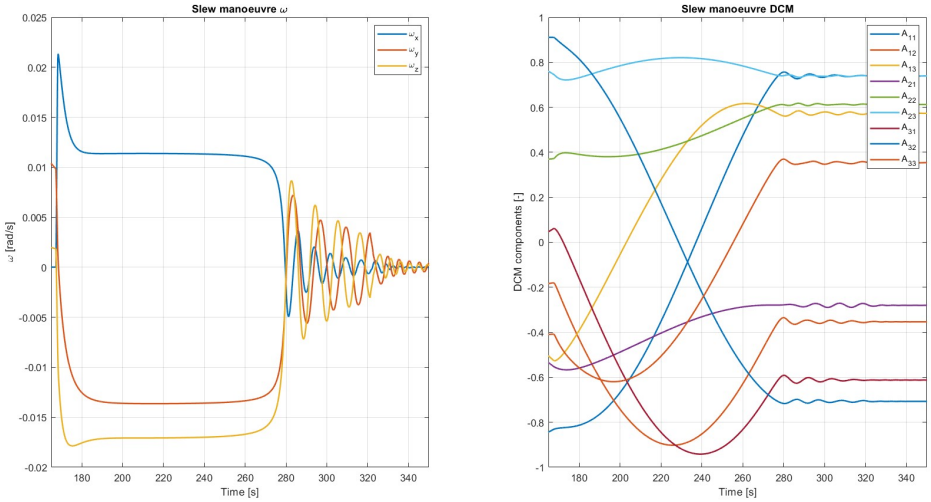

Figure 18: ω and DCM components variation during the slew manoeuvre

9 Conclusion

In the presented project the model for a 6U cubesat pointing mission is implemented. The goal of the mission is to point towards Aldebaran, a star in the Taurus constellation, during the eclipse phase of the spacecraft orbit.
The spacecraft is able to work in five different phases (Star pointing, Sun pointing, Earth pointing, Detumbling, Desaturation if requested) changing the target pointing using a Proportional-Derivative control action. The ASTERIA 6U cubesat reaches high performance in pointing precision, around 30 arcseconds during the standard star pointing. While using piezoelectric actuators it increases the performance up to 5 arcseconds of pointing error [2]. The spacecraft modeled in this project has a request performance in terms of pointing error of 1 arcminute during the star observation phase, 1 degree during the sun pointing and 5 degrees during the Earth pointing phase (figure 19). The star pointing goal is almost achieved (figure 19a) in fact there are only some moments in 75 minutes of observation that the error of spacecraft is higher than one arcminute. The sun pointing goal is overreached (figure 19b), whether the requested power is too high the control during the sun pointing phase might be reduced. The earth pointing goal is perfectly reached (figure 19c), allowing the transmission of the acquired data to the ground station. During the third pointing phase study the y body axis follows the target but for the other two axes the error is larger, a further improvement in the control might reduce the error.
The spacecraft high elliptical orbit improves the performances and allows a longer observation of the star but the apocentre is in the shadow cone only for part of the year, limiting the operativity of the cubesat. A further optimization of the problem is the analysis of a Sun-syncronous orbit to keep the apocentre in the Earth shadow cone during an entire year, to increase the number of the observable stars.

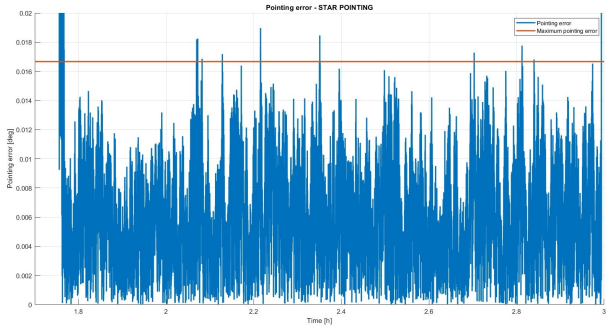

(a) Star pointing error

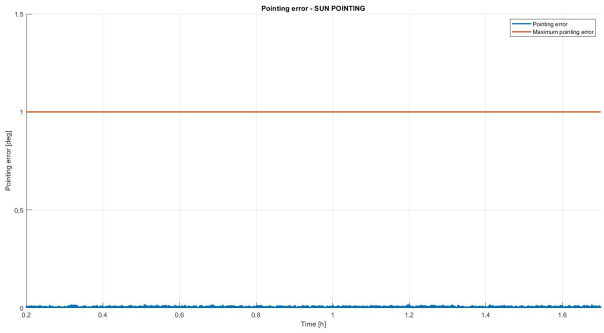

(b) Sun pointing error

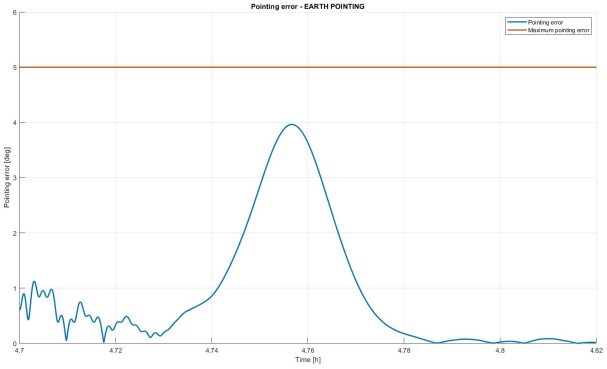

(c) Earth pointing error

Figure 19: Spacecraft pointing performances

References

[1] Mary Knapp et all. "Demonstrating High-precision Photometry with a CubeSat: ASTERIA Observations of 55 Cancri e". In: *The Astronomical Journal* (2020).

[2] Christopher M. Pong. "On-Orbit Performance and Operation of the Attitude and Pointing Control Subsystems on ASTERIA". In: *Jet Propulsion Laboratory* (2018).

[3] Alessandra Babuscia et all. "Arcsecond Space Telescope Enabling Research in Astrophysics Telecommunications". In: *Jet Propulsion Laboratory* (2019).

[4] KLK. *NanoTorque GSW-600 Datasheet.* 2018.

[5] Fizoptika Malta. *Fiber obtic gyroscope VG103S-2LND Datasheet.* 2022.

[6] Blue Canyon technologies. *Star sensor standard NST.*

[7] Katja Reicher et all. "Precise radial velocities of giant stars". In: *Astronomy & Astrophysics* (2019).

[8] A.P.Hatzes et all. "Long-lived, long-period radial velocity variations in Aldebaran: A planetary companion and stellar activity". In: *Astronomy & Astrophysics* (2015).

[9] IGRF. "International Geomagnetic Reference Field". In: (2020).

[10] Safran. *Fiber optic gyroscope Stim 300 Datasheet.*